# The isotropic spectrum of the CO2 Raman 2 nu(3) overtone: A line-mixing band shape analysis at pressures up to several tens of atmospheres

I.-A. Verzhbitskiy, A.-P. Kouzov, Florent Rachet, Michel Chrysos

AIP | The Journal of Chemical Physics

# The isotropic spectrum of the CO2 Raman 2v3 overtone: A line-mixing band shape analysis at pressures up to several tens of atmospheres

I. A. Verzhbitskiy, A. P. Kouzov, F. Rachet, and M. Chrysos

Citation: The Journal of Chemical Physics **134**, 224301 (2011); doi: 10.1063/1.3596750
View online: http://dx.doi.org/10.1063/1.3596750
View Table of Contents: http://scitation.aip.org/content/aip/journal/jcp/134/22?ver=pdfcov
Published by the AIP Publishing



# The isotropic spectrum of the $CO_2$ Raman $2\nu_3$ overtone: A line-mixing band shape analysis at pressures up to several tens of atmospheres

I. A. Verzhbitskiy,[1] A. P. Kouzov,[2] F. Rachet,[1] and M. Chrysos[1,a)]
[1]*MolTech-Anjou, UMR CNRS 6200, Université d'Angers, 2 boulevard Lavoisier, 49045 Angers, France*
[2]*Institute of Physics, Saint Petersburg State University, Ulyanovskaya str. 1, Peterhof, Saint Petersburg 198504, Russia*

(Received 8 April 2011; accepted 12 May 2011; published online 9 June 2011)

A line-mixing shape analysis of the isotropic remnant Raman spectrum of the $2\nu_3$ overtone of $CO_2$ is reported at room temperature and for densities, $\rho$, rising up to tens of amagats. The analysis, experimental and theoretical, employs tools of non-resonant light scattering spectroscopy and uses the extended strong collision model (ESCM) to simulate the strong line mixing effects and to evidence motional narrowing. Excellent agreement at any pressure is observed between the calculated spectra and our experiment, which, along with the easy numerical implementation of the ESCM, makes this model stand out clearly above other semiempirical models for band shape calculations. The hitherto undefined, explicit $\rho$-dependence of the vibrational relaxation rate is given. Our study intends to improve the understanding of pressure-induced phenomena in a gas that is still in the forefront of the news. © *2011 American Institute of Physics*. [doi:10.1063/1.3596750]

## I. INTRODUCTION

A wide variety of absorption or scattering band shapes exist and their analysis can be used to uncover the electro-optical properties of the material on the microscopic level. Not only can such devices be used as sensitive probes of the local molecular environment, they can also help one to get an accurate view of how the particles in condensed systems evolve in the phase space as they absorb, store, or scatter radiation. Whereas, at low pressures, the spectra exhibit a reasonably well-resolved rotational structure, the lines are so broadened at higher pressures that they merge into one another and into the general background. Peculiar effects may occur at such regimes. Among such, it is worth mentioning the line mixing, the band shift or broadening, or the surprising motional narrowing effect, an effect consisting in the narrowing of the resonance line of a system upon increase of the fluctuations of the bath to which the system is coupled.

Anderson's paper is a milestone in the history of band shape modeling.[1] Lots of seminal papers followed his work. The Refs. 2–8 are only a general survey of a topic in which serious attempts have been made over the years to analyze and interpret collisional spectrum broadening, narrowing, or shifting effects. The demand for accurate spectral data worldwide stemming from combined theoretical and experimental studies is higher now than ever before. Such information is in great request in various scientific and industrial fields for numerous gases and mixtures. In this respect, carbon dioxide is one of the topics that have caught the most attention from scientists in the recent years.[9] In an article about near-IR spectra by solid mixtures of $CO_2$ with $H_2O$ and $CH_3OH$, scientists from NASA (Ref. 10) have suggested that the $2\nu_3$ overtone of carbon dioxide would be "*a good observational (spectral) indicator of whether solid $CO_2$ is a pure material or intimately mixed with other molecules.*" Yet, the exhaustive band shape analysis of the $2\nu_3$ band of $CO_2$ still remains unaccomplished.

The purpose of this article is to report, analyze, and interpret the shape of the isotropic component of the $2\nu_3$ overtone of $CO_2$ at various gas densities. The article is in the continuation of a series of recent works by the authors. In that saga, the first work was devoted to the symmetry properties of vibrational stretching in centrosymmetric molecules, in conjunction with the polarization properties of the scattered radiation.[11] Experimental evidence of the almost fully depolarized character of the $2\nu_3$ overtone of $CO_2$ was given therein, along with a spectral moment analysis accounting for electro-optical and mechanical anharmonicity effects and for intermode couplings. So too was the case with our subsequent article, in which a very feeble isotropic spectrum was evidenced for that overtone, and then reported and interpreted; the intensity of its spectrum was found to be some 40 times weaker than the intensity of the dominant anisotropic component, and the agreement between the theoretical predictions and the observation was excellent.[12] In an even more recent article, a successful band shape analysis was made for the anisotropic spectrum, for various $CO_2$ pressures rising up to 55 amagat.[13]

Now, in the new investigation, we go one step forward, providing the reader with the even subtler band shape analysis of carbon dioxide's remnant trace Raman spectrum of $2\nu_3$. Unlike our preceding paper, the modeling of that spectrum now permits to shed more light on pressure effects, especially with respect to vibrational broadening, and to give the exact way in which the vibrational shift and width scale, for that spectrum, with the $CO_2$ density.

a)Electronic mail: michel.chrysos@univ-angers.fr.

 

## II. EXPERIMENTAL

The spectral shapes were recorded at room temperature ($T = 294.5$ K), over a wide range of Raman frequency shift (4515–4810 $cm^{-1}$) and gas density (5–55 amagat).[14] As excitation light source, the green $Ar^+$ laser spectral line ($\lambda_L = 514.5$ nm) was used, whose polarization is by default perpendicular to the scattering plane. This $\perp$-polarized incident beam permitted the recording of the $S_\perp$ scattering signal. The $S_\parallel$ signal was measured by switching the polarization of the beam from the $\perp$ to the $\parallel$ direction. For both signals, high-sensitivity detectors were used; exhaustive description of the detectors and of the experimental setup can be found elsewhere.[15] The isotropic signal, $S^{iso}$, was obtained as a linear combination of $S_\perp$ and $S_\parallel$, implying a delicate subtraction of the $S_\parallel$ component, after application of appropriate weighting factors for setup geometry and scattering beam aperture.[12] The integrated signal of the isotropic spectrum was found to behave strictly linearly with the gas density $\rho$ over the whole density range. This observation is compelling indication that the recorded band stems from intramolecular transitions alone rather than intermolecular transitions implying the presence of Raman-active supermolecular $(CO_2)_n$ $(n > 1)$ clusters.

## III. THEORY

### A. Allowed Raman line positions

Unlike the anisotropic spectrum, which has a three-fold —O, Q, S— branch structure, the isotropic spectrum obeys the selection rule $\Delta J = 0$ and has only a branch Q. The frequency of each of its constituent Raman rotational lines can be found from the following equation:[16]

$$\nu_J = \nu_{00} + \Delta B J(J+1) - \Delta D [J(J+1)]^2 + \Delta H [J(J+1)]^3 . \quad (1)$$

Here, $J$ is the rotational quantum number for this transition and $\nu_{00}$ is the vibrational frequency of $v' \leftarrow v(J = 0)$. Quantities $\Delta B$, $\Delta D$, and $\Delta H$ denote $B' - B$, $D' - D$, and $H' - H$, respectively, where $B$, $D$, and $H$ ($B'$, $D'$, and $H'$) denote the spectroscopic constants for the initial (final) vibrational state. The values of these constants for the $00^02 \leftarrow 00^00$ transition of $^{12}C^{16}O_2$ were taken from the HIgh resolution TRANsmission (HITRAN) database.[17] Table I gathers these values along with the value of $\nu_{00}$ in $cm^{-1}$.

Together with the band of the $00^02 \leftarrow 00^00$ transition, another band, centered at 4648 $cm^{-1}$, occurs due to the hot transition $01^12 \leftarrow 01^10$. The latter band splits up, because of $l$-doubling, into two sub-bands, $e$ and $f$. The sub-bands are distinguished by the parity of $J$, and each of the lines is labeled by the odd or even $J$ value that is associated therewith, respectively. Each of these sub-bands has its own spectroscopic constants.[17] Their values are collected in Table II.

TABLE I. Spectroscopic constants (in $cm^{-1}$), relevant to this study, for the $00^02 \leftarrow 00^00$ transition of $^{12}C^{16}O_2$.

| $\nu_{00}$ ($cm^{-1}$) | $B$ ($cm^{-1}$) | $\Delta B$ ($cm^{-1}$) |
|---|---|---|
| 4673.325 369 9(112) | 0.390 218 949(36) | −0.006 152 802(37) |
| | $\Delta D$ ($10^{-6}$ $cm^{-1}$) | $\Delta H$ ($10^{-12}$ $cm^{-1}$) |
| | −0.000 707 03(1956) | −0.004 172(2714) |

TABLE II. Spectroscopic constants (in $cm^{-1}$), relevant to this study, for the "hot"transition $01^12 \leftarrow 01^10$ of $^{12}C^{16}O_2$.

| | $\nu_{00}$ ($cm^{-1}$) | $B$ ($cm^{-1}$) | $\Delta B$ ($cm^{-1}$) |
|---|---|---|---|
| $e$ | 4648.333 303 1(91) | 0.390 639 109(15) | −0.006 091 675(25) |
| $f$ | 4648.333 303 1(91) | 0.391 254 698(20) | −0.006 125 709(46) |
| | | $\Delta D$ ($10^{-6}$ $cm^{-1}$) | |
| $e$ | | −0.001 199 3(160) | |
| $f$ | | 0.000 017 9(420) | |

### B. Allowed Raman line intensities

The strengths of the rotational lines $J$ that compose a Raman-active isotropic band are given, in $cm^2$ units, by the expression

$$I_J = k_s^4 P_J |\langle \Psi_{v',0} | \bar{\alpha} | \Psi_{v,0} \rangle|^2 = k_s^4 g_J (2J+1) Z^{-1} e^{-\frac{E_v}{k_B T}} |\langle \Psi_{v',0} | \bar{\alpha} | \Psi_{v,0} \rangle|^2 . \quad (2)$$

Here, $k_s (= 2\pi/\lambda_s = 2\pi\nu_s)$ is the norm of the scattered wave vector, with $\nu_s = \nu_L - \nu_J$ and $\nu_L (= \lambda_L^{-1})$ the laser wave number; $\bar{\alpha}$ is the mean polarizability of the molecule; $\Psi_{v,0}$ ($\Psi_{v',0}$) denotes the wave function of the initial (final) vibrational state; $P_J$ designates the population of the initial vibrational state $(E_v, J)$; and $Z$ is the partition function; classically, $Z = k_B T/2B$. Finally, $g_J$ denotes statistical weighting factors for rotational lines; in $CO_2$, even $J$ values have $g_J = 1$ and odd $J$ values have $g_J = 0$, so the odd-parity rotational lines should, in principle, be entirely absent in this molecule. However, in the presence of $l$-doubling, this symmetry property does not hold anymore, so the hot band exhibits both odd and even $J$ values. These two parities manifest themselves in the form of the two distinct sub-bands, $e$ and $f$, respectively.

According to the description made above, there are three distinct vibrational transitions, all compatible with the selection rule $\Delta J = 0$ and nearly equal energetically. They generate three individual Q branches, located in the same frequency domain, which all pertain to the $2\nu_3$ overtone. The main branch, dominant by far (93%), comes from the transition $00^02 \leftarrow 00^00$. It is centered at 4673 $cm^{-1}$. The other two branches are those due to the hot transition $01^12 \leftarrow 01^10$. They are red-shifted by about 25 $cm^{-1}$ from the value 4673 $cm^{-1}$ and share the residual intensity equally ($2 \times 3.5\%$).

Figure 1 shows, in a stick spectrum, the strengths of all the three branches, properly scaled and normalized $(c_J/\Sigma_J c_J)$, against line frequencies $\nu_J$. The spectrum was derived by applying Eqs (1) and (2).

### C. Band shape modeling

Amongst the approaches that are actively employed to calculate a spectrum, the Fano-Mori projection is a very useful and elegant one.[18] Basically, this approach consists in

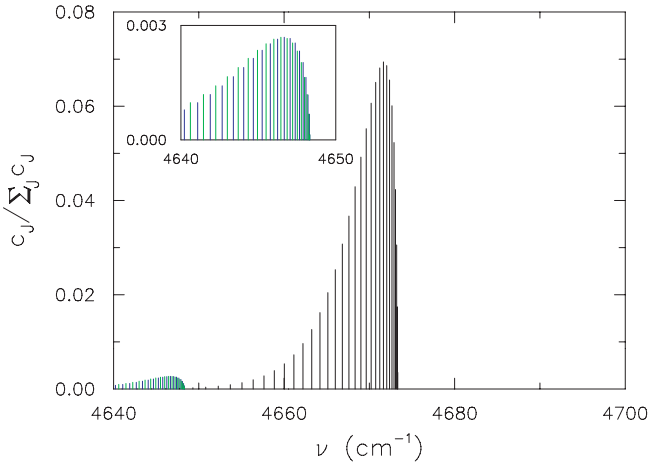


FIG. 1. Stick spectrum of the $2\nu_3$ overtone isotropic component. In addition to the $00^02 \leftarrow 00^00$ transition of interest, the hitherto hidden contribution of the hot transition $01^12 \leftarrow 01^10$ is now clearly visible. The horizontal axis represents Raman shift, $\nu$, in units of $cm^{-1}$. The vertical axis represents intensity $c_J/\Sigma_J c_J$ (no units) and $c_J$ s are line $\delta$-function strengths. The spectrum is unit normalized. The slight prominence at the left of the figure is the hot band. A zoom into this region is shown in the inset. The blue (dark grey) and green (light grey) sticks represent sub-band $e$ and sub-band $f$, respectively.

averaging the effect of the bath on the time evolution of the relevant transition operator $A$. As a result, linearly correlated matrix elements $(A)_{fi} = \langle f | A | i \rangle$ are obtained for transitions $f \leftarrow i$ that are optically allowed in the free molecule. In the remainder of this article, the symbol $A_m$ will be adopted to denote $(A)_{fi}$, where $m$ is an index numbering the transitions. The transitions are thus considered as elements, $|m\rangle\rangle$, of a line space in which transition frequencies $\omega_m (= \omega_{fi})$ are eigenvalues of the free-molecule Liouville operator, $\hat{L}\,|m\rangle\rangle = \omega_m\,|m\rangle\rangle$. The resulting spectrum function reads

$$\Phi(\omega) = \frac{1}{\pi}\mathrm{Re}\sum_{m,m'} A_m A_{m'} \left\{[-i\,(\omega\mathbf{I} - \mathbf{L}) + \mathbf{\Gamma}]^{-1}\right\}_{m,m'}. \quad (3)$$

The bold characters in this expression were used to denote matrices; $\mathbf{\Gamma}$ stands for the relaxation matrix; $\mathbf{L}$ stands for the Liouville matrix; $\mathbf{I}$ is the identity matrix; and $A_m^2$ has the meaning of integrated intensity of line $m$. Here, $\Delta J = 0$, so $m = J$ . In what follows, we will assume the band intensity to be unit normalized, i.e., $\sum_m A_m^2 = 1$. Also, we will neglect for a while the vibrational part of $\mathbf{\Gamma}$ trying to concentrate on the rotational part.

In the Markov approximation, which remains valid for the purposes of this study, $\mathbf{\Gamma}$ is a quantity that does not depend on frequency. If, moreover, the off-diagonal elements of $\mathbf{\Gamma}$ are neglected (isolated line approach), the previous expression is reduced to a simple sum of Lorentzians,

$$\Phi(\omega) = \frac{1}{\pi}\sum_m A_m^2 \frac{\gamma_m}{(\omega - \omega_m - \delta_m)^2 + \gamma_m^2}, \quad (4)$$

each of which is shifted from $\omega_m$ by $\delta_m = \mathrm{Im}\Gamma_{m,m}$ and has a half-width at half-maximum (HWHM) equal to $\gamma_m = \mathrm{Re}\Gamma_{m,m}$.

We will henceforward assume that the line shifts $\delta_m$ (usually much smaller than the line widths $\gamma_m$) are negligible. This model will be referred to as A.

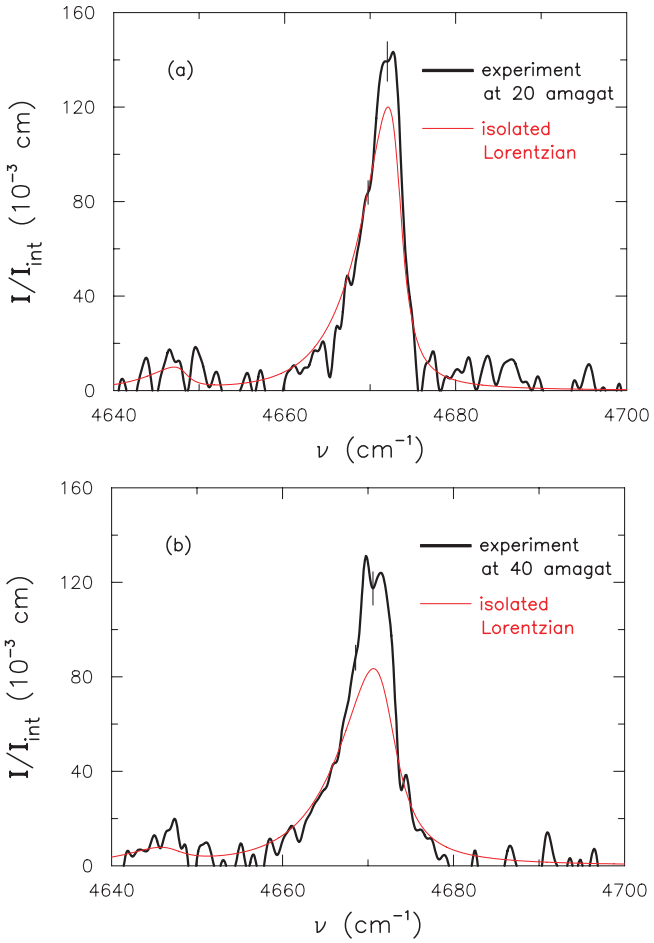


FIG. 2. Calculated [thin red (thin light grey) line] and recorded [thick black (thick dark grey) line] spectrum intensities $I/I_{int} (= I/\int I d\nu)$ in cm units, as a function of Raman shift, $\nu$, in units of $cm^{-1}$. Model A was employed for the calculations. The gas temperature is 294.5 K. The gas density is: 20 amagat (a) and 40 amagat (b). The spectra are unit normalized. Vertical bars are used to show the experimental error.

Figure 2 shows the theoretical spectrum as it was calculated with model A in comparison with the experimental one. The spectra are unit normalized. The abscissa represents Raman frequency shift in $cm^{-1}$ units. The densities are 20 and 40 amagat. Because of the short separation between rotational lines, the coalescence occurs early in the collision process. As a result, the rotational structure was invisible from the spectra even at the lowest gas density. A dramatic divergence, which is particularly clear at the central frequency region of the Q branch, is observed between the response of model A and the measured spectra, with the discrepancies being more and more apparent as density is increased. The missing intensity in the central part is due to the incomplete intensity transfer from the wings of the band to the center. This transfer lies with line mixing, an effect disregarded in the framework of A. The insufficiency of this model to capture the evolution of the band shape, as gas density is increased, is clear from these figures.

In fact, as a consequence of the heavy line mixing, a single quasi Lorentzian line starts to be built up immediately after the first signs of coalescence have appeared in the rotational structure. The width of this line turns out to decrease as the gas density is increased, which is the very signature

of "motional narrowing." Here, this effect was masked by the more pronounced vibrational band broadening, $\gamma_\upsilon$, which rendered the direct detection of motional narrowing impossible in $CO_2$ (see also footnote[19]). Nevertheless, a simulation with the $\gamma_\upsilon$ parameter being artificially "switched off" was conducted, and it was used as a means to see indirectly this intriguing effect; the thorough description of this numerical experiment is made at the end of this paper.

In what follows, we will assume that all the changes in the spectrum occur within the binary collision regime in which $\mathbf{\Gamma}$ scales linearly with density $\rho$. The validity of this assumption will be confirmed *a posteriori* in this article, by the striking agreement that we eventually observed between theory and experiment (see below).

### 1. The motional narrowing

The simplest way to evidence motional narrowing theoretically is by applying the so-called memory function formalism.[18] In this formalism, the spectral function is associated with a memory function, $M(\omega)$, through the expression

$$\Phi(\omega) = \frac{1}{\pi}\mathrm{Re}\left[-i(\omega - \Omega) + M(\omega)\right]^{-1}, \tag{5}$$

where $\Omega$ $[= \langle\langle A\,|\mathbf{L_T}|\,A\rangle\rangle]$ is the mean frequency of the band and $\mathbf{L_T}$ the total Liouvillian.

It has been shown by Kouzov[20] that, in this formalism, $M(\omega)$ can be obtained by introducing the projector $\mathbf{P}_A = |A\rangle\rangle\langle\langle A|$ on the normalized vector $|A\rangle\rangle$. After tedious algebra and appropriate application of the sum rules,[21,22] the following compact expression is obtained:

$$M(\omega) = i\langle\langle B|[\omega - Q_A\mathbf{L_T}Q_A + iQ_A\mathbf{\Gamma}Q_A]^{-1}|B\rangle\rangle, \tag{6}$$

with $|B\rangle\rangle = |Q_A\mathbf{L_T}A\rangle\rangle = |(\mathbf{L_T} - \Omega)A\rangle\rangle$ and $Q_A = 1 - \mathbf{P}_A$.

Clearly, upon inspection of Eqs. (5)(6), at pressures that are high enough, i.e., for $|\Gamma| \gg |L_T - \omega|$, the memory function is reduced to a constant

$$M(\omega) \underset{|\Gamma|\gg|L_T-\omega|}{\longrightarrow} \langle\langle B|(Q_A\mathbf{\Gamma}Q_A)^{-1}|B\rangle\rangle = \Gamma_{\frac{1}{2}}, \tag{7}$$

so the band shape degenerates to a Lorentzian function with HWHM equal to $\Gamma_{\frac{1}{2}}$. Since $\Gamma_{\frac{1}{2}}$ is inversely proportional to density, the band profile grows up and narrows in as $\rho$ is increased; this is exactly what motional narrowing means for a spectrum.

### 2. The extended strong collision model

The interesting specific properties of the projector operator have allowed Kouzov[20] to work out, within the earlier proposed[23] ESCM, an analytical expression for the spectrum function. In contrast with the definition $\Gamma_{m,m'} = \Gamma(\delta_{m,m'} - A_m A_{m'})$ ($\Gamma$ is a constant) used in the rather conventional strong collision model (SCM), within the ESCM the relaxation matrix elements read

$$\Gamma_{m,m'} = \gamma'_m\left(\delta_{m,m'} - \frac{\gamma'_{m'}}{\langle\gamma'\rangle}A_m A_{m'}\right). \tag{8}$$

In this expression, a "broadening mean value" $\langle\gamma'\rangle$ $[= \sum_m A_m^2\gamma'_m]$ is introduced to ensure fulfillment of the sum rules.[21,22] Primes are used to distinguish the elements $\gamma'_m$ from the experimental line widths $\gamma_m(= \Gamma_{m,m})$. Since typical spectra obey $A_m^2 \ll 1$, the quantities $\gamma'_m$ only slightly differ from $\gamma_m$, so the calculation of the primed elements can be readily done within few iterations out of the unprimed ones. In this way, an exact description of the band shape can be made at any pressure.

The ESCM relaxation matrix can be written in a more compact way, as

$$\mathbf{\Gamma} = \boldsymbol{\gamma}' - \frac{|\boldsymbol{\gamma}'A\rangle\rangle\langle\langle\boldsymbol{\gamma}'A|}{\langle\gamma'\rangle}, \tag{9}$$

where the second term has the meaning of a projector onto the vector $|\boldsymbol{\gamma}'A\rangle\rangle$; $\boldsymbol{\gamma}'$ is a diagonal matrix whose diagonal elements are the effective widths $\gamma'_m$. Thanks to the projector-like form of the off-diagonal part of this expression, a great simplification in the calculation of $\Phi(\omega)$ is possible and the final result reads[20]

$$\Phi(\omega) = \frac{1}{\pi}\mathrm{Re}\left[\left\langle\left\langle A\left|\mathbf{R}_d^{-1}\right|A\right\rangle\right\rangle + \frac{\left\langle\left\langle A\left|\mathbf{R}_d^{-1}\boldsymbol{\gamma}'\right|A\right\rangle\right\rangle^2}{\langle\gamma'\rangle - \left\langle\left\langle A\left|\mathbf{R}_d^{-1}\boldsymbol{\gamma}'^2\right|A\right\rangle\right\rangle}\right]. \tag{10}$$

In this expression, $\mathbf{R}_d$ denotes the diagonal matrix $\mathbf{R}_d = -i(\omega\mathbf{I} - \mathbf{L}) + \boldsymbol{\gamma}'$. Inverse of this matrix in the line space is trivial.

The model of Eq. (10) will be referred to as B.

## IV. RESULTS AND DISCUSSION

A FORTRAN code was written for the calculation of the band shape from Eq. (10). As input rotational broadening coefficients, HITRAN data, calculated with the Robert-Bonamy semi-classical model, were used.[24]

A careful shape analysis showed that the vibrational component of the pressure effects had too significant an impact on the shape to be ignored. Although the way to account for those missing effects may not be obvious at the outset, the suggestion was made in this paper that rotational and vibrational relaxation channels should be completely decoupled. This assumption, which is dictated by the property of statistical independence, offers a simple but effective means to solve the problem. Practically, these effects were taken into account in the calculation by simply changing $\omega$ to $\omega + i(\gamma_\upsilon + i\delta_\upsilon)$, in the expression of $\mathbf{R}_d$ [Eq. (10)]. The parameter $\gamma_\upsilon + i\delta_\upsilon$ was used*ad hoc* to describe vibrational broadening and shift. As before with model A, Markov's approximation was used.

We recall that, in our preceding work on the anisotropic spectrum,[13] no $\gamma_\upsilon/\rho$ value was reported, even though an accurate value for $\delta_\upsilon/\rho$ equal to $-0.034(3)$ $\mathrm{cm}^{-1}$/amagat could be extracted from that spectrum. In fact, the vibrational broadening, in that spectrum, was so masked by the far more substantial rotational line broadening that $\gamma_\upsilon/\rho$ was entirely undetectable on the reported shapes. This is no longer the case with the isotropic spectrum, which (in contrast with its anisotropic counterpart) is a powerful tool for accessing, at high gas pressures, the parameter $\gamma_\upsilon/\rho$. Interestingly, this possibility is because of motional narrowing: At high gas

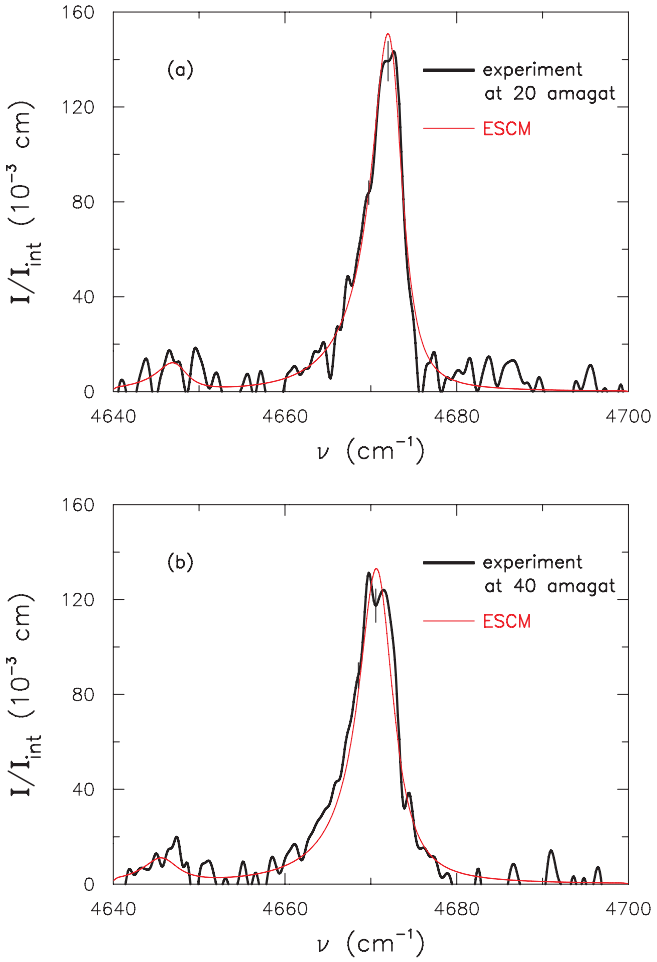


FIG. 3. Same as in Fig. 2 but for model B (ESCM).

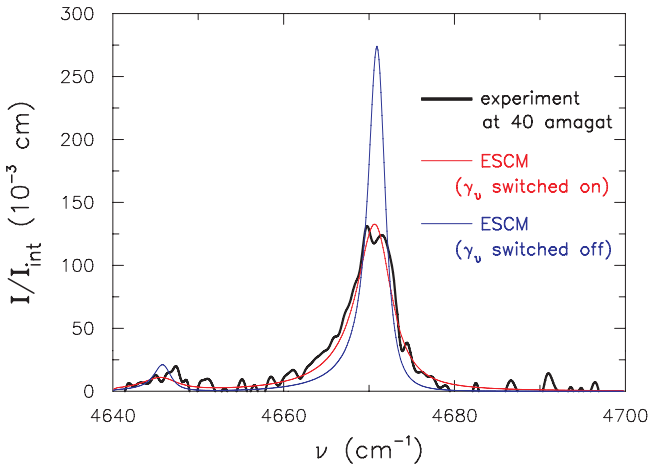


FIG. 4. Calculated spectrum intensities $I/I_{int}(= I/\int I d\nu)$ in cm units, as a function of Raman shift, $\nu$, in units of $cm^{-1}$. The red line (smooth flat curve) represents the spectrum computed after proper inclusion of $\gamma_\upsilon$. The blue line (smooth sharp curve) represents the spectrum computed with $\gamma_\upsilon = 0$. The thick black line (unsmooth flat curve) is the recorded spectrum. Model B (ESCM) was employed for the calculations. The gas temperature is 294.5 K. The gas density is 40 amagat. The spectra are unit normalized.

pressures, rotational line broadening effects in the isotropic spectrum are washed out because of motional narrowing with the cancellation becoming better and better on increasing $\rho$. This interesting property offers an opportunity to extract accurate values for the vibrational relaxation rates from the measured band shapes.

Accurate $\gamma_\upsilon/\rho$ and $\delta_\upsilon/\rho$ values were derived by (least-square) fitting the calculated ESCM shapes [Eq. (10)] to the experimental ones

$$\frac{\gamma_\upsilon}{\rho} = 0.037(2)\ \text{cm}^{-1}/\text{amagat},$$
$$\frac{\delta_\upsilon}{\rho} = -0.037(6)\ \text{cm}^{-1}/\text{amagat}. \quad (11)$$

These two parameters were the only adjustable parameters of this work. Note that the $\delta_\upsilon/\rho$ value of Eq. (11) coincides with the value $-0.034(3)$ $cm^{-1}$/amagat of our preceding paper[13] to within the experimental uncertainty. This observation lends additional credence to its physical relevance. A 0.7 $cm^{-1}$ FWHM triangular function was used to mimic the slit function of the experiment.

Figure 3 shows the ESCM band shapes in comparison with the experimental ones as a function of Raman frequency shift. The gas densities are 20 and 40 amagat. The perfect response of the ESCM is clear from the figures. The agreement between the calculated and the measured shapes is striking and it was found to persist at all densities. This is evidence of the superiority of the ESCM for band shape modeling.

Figure 4 shows the ESCM band shape at 40 amagat with and without inclusion of $\gamma_\upsilon$ in the simulation. This illustration permits to showcase the importance of vibrational broadening at the high density regime and, by this very fact, to show off how strong the motional narrowing was at those densities. It is clear from this figure that, in the absence of vibrational broadening, the band shape appears to be significantly narrower and stronger than the actual band shape. Thus, not only is that observation evidence of a very strong vibrational broadening in the spectrum, it is also the evidence of a pronounced motional narrowing in agreement with the theoretical predictions of Eqs. (5)–(7).

It is worth pointing out that both $\gamma_\upsilon/\rho$ and $-\delta_\upsilon/\rho$ take values [Eq. (11)] that are several times greater than those known for the vibrational relaxation parameters of the $CO_2$ doublet $\nu_1 : 2\nu_2^0$ Fermi resonance components (see Ref. 25 and references therein). Specifically, the $\gamma_\upsilon/\rho$ coefficients reported in Ref. 25 for the 1388 and 1285 $cm^{-1}$ $\nu_1 : 2\nu_2^0$ components amount to 0.0038(1) and 0.0057(1) $cm^{-1}$/amagat, respectively; as for the corresponding $-\delta_\upsilon/\rho$, they amount to $\approx 0.005$ and 0.01 $cm^{-1}$/amagat, respectively. To the best of our knowledge, these four values still remain the only data available to date for vibrational relaxation parameters in fundamental $CO_2$ bands.

Although the rigorous explanation of the here-reported amplification of the $\gamma_\upsilon/\rho$ and $-\delta_\upsilon/\rho$ values, on going from a fundamental band to the $2\nu_3$ overtone, is a vast and arduous task, this result was well expected qualitatively. Two reasons can be invoked to explain this observation:

(1) The treatment, with perturbation theory, of the transition matrix elements predicts the dephasing part of the broadening to scale quadratically with the difference $\upsilon' - \upsilon$ between the initial and final vibrational quantum numbers.[26] As

a result, bands by first overtones are expected to be four times as broadened as bands by fundamental transitions.

(2) The $\nu_3$ vibration is reputed to have a large transition dipole moment.[27] Such a large value opens up a second channel of broadening, which is due to the vibrational energy exchange. The exchange rate is enhanced even more on going from the fundamental transition to the overtone.

Unfortunately, the measurements of the IR $\nu_3$ fundamental band are not sensitive enough to allow one to reliably determine vibrational broadening. Besides, no data exist to check the $(\upsilon' - \upsilon)^2$ scaling law in the case treated in the present paper.

Before closing this paper, let us make a comment about the fluctuations of the experimental profiles of Figs. 2 and 3. It is a general property of isotropic Raman intensity recordings to be more noisy than depolarized ones. The origin of this additional component of noise is inherent in operations of subtraction $S^{iso} = S_\perp - 7/6\, S_\parallel$; in the present case, the latter operation resulted in fluctuations by about ±6% of the experimental integrated isotropic intensity. To illustrate the experimental error vertical bars were used on Figs. 2 and 3. Interestingly, the fact that the transition $00^02 \leftarrow 00^00$ (along with the transition $01^12 \leftarrow 01^10$), treated in this article, was Raman-allowed made signals $S_\parallel$ and $S_\perp$ to be much stronger than typical collision-induced band signals. (For a comparison see, Refs. 28–30) This property ensured, already from the outset, high quality recordings for $S_\parallel$ and $S_\perp$. Besides, the exceptional property of the depolarization ratio of $2\nu_3$ to be nearly $\nu$-independent,[11] clearly explains why the extraction procedure $S^{iso} = S_\perp - \frac{7}{6} S_\parallel$ was that much reliable for that overtone. Incidentally, our measured moment for the isotropic spectrum $[M_0^{iso}(\text{ expt}) = 9.1(6) \times 10^{-6}\ a_0^6]$ has already been shown to be in excellent agreement with theoretical predictions $[M_0^{iso}(\text{theory}) = 8.4 \times 10^{-6} a_0^6]$,[12] provided that high-quality *ab initio* data[31,32] for the mechanical and electro-optical anharmonicity and couplings were incorporated to properly account for the heavy mixing between the modes $\nu_1$ and $\nu_3$.

## V. SYNOPSIS

This article is in the continuation of our recent study on the band shapes of overtone transitions. We reported a line-mixing shape analysis of the isotropic remnant Raman spectrum of the $2\nu_3$ overtone of $CO_2$ at room temperature and for pressures rising up to near 50 atm. The ESCM was applied to simulate the strong line mixing effects and to evidence motional narrowing. The agreement between the calculated spectra and our experiment was excellent and permitted extraction of the as-of-yet undefined vibrational relaxation rates [Eq. (11)]. This response (see Fig. 3) is to be contrasted with the inadequacy of simpler models, which produce spectra that strongly deviate from the experiment at high gas pressures (see Fig. 2) and are incapable of providing information on the vibrational relaxation. The success of the ESCM and its simplicity make this model stand out clearly above other semiempirical models for band shape calculations in the effort to interpret high-sensitivity non-resonant light scattering experiments. Our study intends to advance the cause of pressure-induced phenomena in greenhouse gases, which are currently receiving an increasing public attention.

## ACKNOWLEDGMENTS

Fruitful discussions with Professor H. W. Schrötter (Ludwig-Maximilians Universität, München) are acknowledged.

[1] P. W. Anderson, Phys. Rev. **76**, 647 (1949).
[2] M. Baranger, Phys. Rev. **111**, 481 (1958).
[3] U. Fano, Phys. Rev. **131**, 259 (1963).
[4] A. Ben-Reuven, Phys. Rev. **145**, 7 (1966).
[5] P. W. Rosenkranz, IEEE Trans. Antennas Propag. **AP-23**, 498 (1975).
[6] A. C. Kolb and H. Griem, Phys. Rev. **111**, 514 (1958).
[7] V. I. Alekseev and I. I. Sobel'man, Zh. Eksp. Teor. Fiz. **55**, 1874 (1969) [Soviet Phys. JETP **28**, 991 (1969)].
[8] J. Bonamy, L. Bonamy, and D. Robert, J. Chem. Phys. **67**, 4441 (1977).
[9] C. E. Miller, L. R. Brown, R. A. Toth, D. C. Benner, and V. M. Devi, C. R. Phys. **6**, 876 (2005).
[10] M. P. Bernstein, D. P. Cruikshank, and S. A. Sandford, Icarus **179**, 527 (2005).
[11] M. Chrysos, I. A. Verzhbitskiy, F. Rachet, and A. P. Kouzov, J. Chem. Phys. **134**, 044318 (2011).
[12] M. Chrysos, I. A. Verzhbitskiy, F. Rachet, and A. P. Kouzov, J. Chem. Phys. **134**, 104310 (2011).
[13] I. A. Verzhbitskiy, A. P. Kouzov, F. Rachet, and M. Chrysos, J. Chem. Phys. **134**, 194305 (2011).
[14] A fuller description of the electro-optical properties of the weak isotropic component, obtained from the experiment, along with a complete comparison of these data with accurate theoretical calculations, can be found in a previous article (Ref. 12).
[15] F. Rachet, Y. Le Duff, C. Guillot-Noël, and M. Chrysos, Phys. Rev. A **61**, 062501 (2000).
[16] G. Herzberg, *Molecular Spectra and Molecular Structure. Part II. Infrared and Raman Spectra of Polyatomic Molecules* (van Nostrand, Princeton, 1966).
[17] C. E. Miller and L. R. Brown, J. Mol. Spectrosc. **228**, 329 (2004).
[18] D. Forster, *Hydrodynamic Fluctuations, Broken Symmetry, and Correlation Functions* (Benjamin, Reading, MA,1975).
[19] Whereas the structural properties of $CO_2$ make the observation of this effect extremely difficult, shorter molecules, such as $N_2$, may exhibit motional narrowing effects directly detectable on the spectrum, owing to the less efficient interplay between the inherent mechanisms of motional narrowing and vibrational broadening.
[20] A. P. Kouzov, Chem. Phys. Lett. **188**, 25 (1992).
[21] N. N. Filippov and M. V. Tonkov, J. Chem. Phys. **108**, 3608 (1998).
[22] Sum rules are fundamental properties for a relaxation matrix, which must always be fulfilled upon performing matrix inversion in the line space. They relate the diagonal part of $\mathbf{\Gamma}$ with its off-diagonal terms, as (Ref. 21) $\sum_{m'} A_{m'} \Gamma_{m,m'} = \sum_m A_m \Gamma_{m,m'} = 0$. For more about these rules, see Ref. 21 as well as our preceding paper (Ref. 13).
[23] J. P. Sala, J. Bonamy, D. Robert, B. Lavorel, G. Millot, and H. Berger, Chem. Phys. **106**, 427 (1986).
[24] L. Rosenmann, J.-M. Hartmann, M. Y. Perrin, and J. Taine, Appl. Opt. **27**, 3902 (1988).
[25] V. Morozov, S. Mochalov, A. Olenin, V. Tunkin, and A. Kouzov, J. Raman Spectrosc. **34**, 983 (2003).
[26] A. P. Kouzov and V. A. Krasheninnikov, Chem. Phys. **126**, 301 (1988).
[27] T. D. Kolomiitsova, A. V. Lyaptsev, and D. N. Shchepkin, Opt. Spectrosc. **88**, 648 (2000).
[28] I. A. Verzhbitskiy, M. Chrysos, F. Rachet, and A. P. Kouzov, Phys. Rev. A **81**, 012702 (2010).
[29] M. Chrysos and I. A. Verzhbitskiy, Phys. Rev. A **81**, 042705 (2010).
[30] I. A. Verzhbitskiy, M. Chrysos, and A. P. Kouzov, Phys. Rev. A **82**, 052701 (2010).
[31] G. Maroulis, Chem. Phys. **291**, 81 (2003).
[32] A. Haskopoulos and G. Maroulis, Chem. Phys. Lett. **417**, 235 (2006).